Numerical Investigation of SiO_2 Coating Deposition in Wafer Processing Reactors with $SiCl_4/O_2/Ar$ Inductively Coupled Plasmas

Stefan Tinck,* Peter De Schepper, Annemie Bogaerts

Simulations and experiments are performed to obtain a better insight in the plasma enhanced chemical vapor deposition process of SiO_2 by $SiCl_4/O_2/Ar$ plasmas for introducing a SiO_2-like coating in wafer processing reactors. Reaction sets describing the plasma and surface chemistry of the $SiCl_4/O_2/Ar$ mixture are presented. Typical calculation results include the bulk plasma characteristics, i.e., electrical properties, species densities, and information on important production and loss processes, as well as the chemical composition of the deposited coating, and the thickness uniformity of the film on all reactor surfaces. The film deposition characteristics, and the trends for varying discharge conditions, are explained based on the plasma behavior, as calculated by the model.

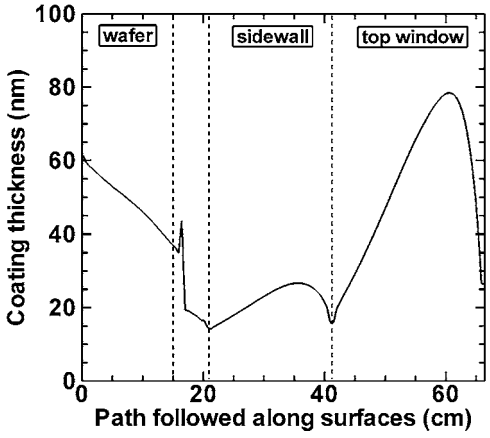

1. Introduction

During wafer processing as applied in the microelectronics industry, it is common to introduce a coating in the reactor chamber before each new processing step.[1] It has been shown that coatings can have beneficial effects in terms of uniformity and wafer-after-wafer process reproducibility.[2,3] During plasma etching, etch products redeposit on the reactor walls, changing the chemical composition of these surfaces, which in turn can significantly affect the discharge properties, such as ion and radical density (e.g., Cl for etching Si), thereby causing process drifts.[3] As a result, a major challenge in integrated circuit processing is to obtain a proper wafer-after-wafer process repeatability.[1] It is therefore common to clean the chamber walls after each wafer processing step, which is typically performed with a SF_6-based plasma to remove $SiCl_xO_y$ species from the walls. However, in this process the (Al_2O_3) walls are converted to AlF_x which can be more easily sputtered in the next plasma step.[1] A solution to this problem is the introduction of a coating (typically SiO_2-like) before the plasma processing step, which is removed afterwards, maintaining similar reactor wall conditions wafer after wafer.

Furthermore, standard inductively coupled plasma (ICP) reactors have Al_2O_3 walls and a quartz top dielectric window. During plasma treatment, the top window is sputtered to some extent due to capacitive coupling from the coil, entailing significant ion bombardment on the quartz plate. The sputtered particles can subsequently redeposit, creating a SiO_2 film on the sidewalls during wafer processing. So, during wafer processing, the reactor walls are slowly becoming covered with SiO_2 sputtered from the quartz plate, changing the wall recombination probabilities of reactive species and hence altering the overall plasma

Dr. S. Tinck, Prof. A. Bogaerts
Research Group PLASMANT, Department of Chemistry, University of Antwerp, Universiteitsplein 1 B-2610, Antwerp, Belgium
E-mail: stefan.tinck@ua.ac.be
P. De Schepper
Interuniversity Microelectronics Centre, Kapeldreef 75 B-3001, Leuven, Belgium

Plasma Process. Polym. **2013,** *10*, 714–730

DOI: 10.1002/ppap.201300005

characteristics. However, if all reactor walls are initially covered with a SiO_2 coating, sputtering of the top window will have minimal influence on the plasma characteristics. Another advantage of applying a SiO_2 coating is that the Cl radical recombination probability is much lower on SiO_2 surfaces, resulting in a higher etch rate on the wafer and improved density uniformity of Cl radicals in chlorine-based etch recipes.[2]

$SiCl_4/O_2$-based plasmas are suitable for introducing SiO_2-like coatings with good chemical and electrical integrity through plasma enhanced chemical vapor deposition (PECVD).[4,5] It has been shown that chlorine-containing gases can be very effective for removing impurities from the reactor walls and for improving the overall chemical and electrical stability of the deposited SiO_2 layer.[6] The basic mechanism of deposition can be summarized as follows: (i) $SiCl_4$ dissociates in the plasma into low- or non-volatile products ($SiCl_{0-3}$) which are the precursor molecules/atoms for deposition. (ii) O_2 and O oxidize the deposited $SiCl_x$-layer to a SiO_2-like layer.[4–7] In addition, the only byproduct is Cl, which can remove H impurities from the SiO_2 layer through formation of HCl.[7]

Several authors have reported on SiO_2 film deposition at low substrate temperature by PECVD using $SiCl_4/O_2$ plasmas. Alonso et al.[6] have experimentally investigated the deposition rate and structural properties of the SiO_2 layer deposited from different $SiCl_4/SiF_4/O_2$ mixtures with ellipsometry, etch rate measurements, and infrared spectroscopy. Ortiz et al.[7] have also used infrared transmittance, Auger electron spectroscopy, ellipsometry, and etch rate measurements to characterize the SiO_2 films deposited through PECVD using $SiCl_4$ and O_2. From their results, it can be concluded that a lower flow of reactant gases results in more homogeneous porous films.

The effect of adding H_2 to the $SiCl_4/O_2$ gas mixture on the properties of SiO_2-like layers has also been experimentally investigated by Alonso et al.[4] They have reported that the addition of H_2 reduces the deposition rate but can improve the stability of the films by reducing the amount of Cl incorporated during growth, due to the formation and extraction of HCl.

Although some work has been carried out already to investigate the chemical and electrical properties of the SiO_2 films deposited by PECVD with $SiCl_4/O_2$-based mixtures, in most cases, experimental measurements are performed in one particular location of the film, yielding limited or no information on uniformity of the deposited layer along the reactor surfaces. However, it is of utmost importance to be able to properly control the deposition uniformity on all reactor surfaces in terms of film thickness and chemical composition. If the chemical state of the SiO_2 coating is not uniform across the reactor surfaces, e.g., if it contains significantly more chlorine in certain locations, the wall recombination probability of radicals such as Cl can be very different, resulting in a less uniform plasma. The same applies to the structural integrity of the coating. If the stability and porosity of the coating show large variations due to a non-uniform deposition rate, sputtering of the coating will create additional local variations in plasma uniformity.

The goal of this paper is therefore to focus on the uniformity of the deposited SiO_2 film along all reactor walls in terms of thickness and chemical state, and to bring insight into how the plasma characteristics determine the coating growth mechanism. For this purpose, a two-dimensional numerical model is applied that can yield information on plasma uniformity as well as on the deposition process at all reactor surfaces for an $Ar/SiCl_4/O_2$ ICP used for PECVD of SiO_2. As mentioned above, $SiCl_4$ is the precursor gas for deposition, while O_2 is the oxidizing agent to create a SiO_2 film. Ar is typically added to dilute the gas for a better control of the deposition rate at a fixed operating pressure and gas flow.

2. Description of the Model

A hybrid Monte Carlo – fluid model is applied to describe the bulk plasma and surface chemistry.[8] A more detailed explanation of the model can be found in this ref.[8]

In this model, an analytical module is included to predict the thickness and chemical composition of the deposited layer on all reactor surfaces during plasma treatment. More specifically, the fluxes from the plasma are used in this module to address the surface processes based on a surface chemistry reaction set. From here, the fluxes of species returning to the plasma, as in the case of etching or sputtering, are defined for an updated description of the plasma behavior. The overall calculation switches between these two parts in an iterative way until convergence is reached.

In the following sections, reaction sets for the bulk plasma and surface chemistry of an $Ar/SiCl_4/O_2$ mixture are presented and discussed.

2.1. Species Considered in the Model

Thirty-two different plasma species are included in the model, as well as nine different surface layers for addressing the wall conditions. The surface layers are denoted by (s). The complete list of species is shown in Table 1.

Electron impact rotational and vibrational excitations are included for Cl_2 and O_2, but not for other molecules. These excited levels of Cl_2 and O_2 are, however, not explicitly taken into account as separate species, but they are included in the ground state species.

Cl_2 consists of the ground state and two electronic excited levels (at 2.49 and 9.25 eV). For these three states, one

Table 1. Overview of the species included in the model.

Ground state neutrals	Ar, Cl_2, Cl, O_2, O, ClO, Si, SiCl, $SiCl_2$, $SiCl_3$, $SiCl_4$, SiO, SiO_2
Positive ions	Ar^+, Cl_2^+, Cl^+, O_2^+, O^+, ClO^+, Si^+, $SiCl^+$, $SiCl_2^+$, $SiCl_3^+$, $SiCl_4^+$, SiO^+, SiO_2^+
Excited species	Ar^*, Cl^*, O^*
Negatively charged species	Cl^-, O^-, electrons
Surface layers	$Si_{(s)}$, $SiCl_{(s)}$, $SiCl_{2(s)}$, $SiCl_{3(s)}$, $SiO_{(s)}$, $SiO_{2(s)}$, $SiClO_{(s)}$, $SiCl_2O_{(s)}$, $SiCl_3O_{(s)}$

vibrational and one rotational excitation are included as well with threshold of 0.07 and 0.02 eV. Similarly, O_2 includes the ground state molecule, and four electronic excited levels (at 0.98, 1.63, 8.40, and 10.00 eV). For these five states, one rotational excitation and two vibrational excitations are also included with thresholds of 0.02, 0.19, and 0.38 eV. For Ar^* a collection of all *4s* levels are lumped together (with defined average threshold of 11.60 eV and all *4p* levels at 13.10 eV. In the same manner, Cl^* comprises of all *4s* (8.90 eV), *3d* (10.40 eV), *4p* (11.80 eV), *4d* (12.00 eV), and 5p (12.40 eV) excited levels, and O^* of the *3s* (9.15 eV) and *3p* (10.73 eV) levels. Other negative ions in our model besides Cl^- and O^- are not included as their densities are negligible.[9–12]

As far as the reaction products are concerned, various Cl_xO_y products might exist in principle, such as ClO, Cl_2O, ClO_2, and Cl_2O_2. However, compared to ClO, other Cl_xO_y products have low densities and therefore only ClO is considered in our model.[13] Finally, it is most likely that $SiCl_xO_y$ species are present in the plasma.[14] However, not much information can be found in literature about the chemical reactions of these species. In ref.[15], it is reported that $SiCl_x$ molecules will only be oxidised in the gas phase at a gas temperature of at least 1 500 *K*, which is much higher than the typical gas temperature under study in this paper (<600 K). Therefore, gas-phase $SiCl_xO_y$ species are not included in our plasma model, but several $SiCl_xO_y$ species are considered in the surface reaction set as surface species.

2.2. Plasma Chemical Reactions Included in the Model

The bulk $SiCl_4/O_2/Ar$ plasma chemistry is decribed by a reaction set which is presented in Table 2. Elastic collisions are included in the model but are not listed in the table. Most electron impact reaction rates are defined by energy dependent cross sections $\sigma(E)$ that can be found in the corresponding references, while in other cases (i.e., some electron impact reactions and all heavy-particle reactions) the reactions are defined by rate coefficients, which are directly presented in the table. Concerning the ion-ion neutralizations, not all rate constants of these combinations are known, but for the typical chemistry under study, these are generally in the order of 10^{-7}–10^{-8} $cm^3 \cdot s^{-1}$. Indeed, for neutralizations between Ar^+ and Cl^- ions, Subramonium and Kushner have provided coefficients which are 10^{-7} $[T/298\,K]^{0.5}$ $cm^3 \cdot s^{-1}$ while Thorsteinsson and Gudmundsson have used a coefficient of 5.00×10^{-8} $[T/298\,K]^{0.5}$ $cm^3 \cdot s^{-1}$ for ion–ion neutralizations between chlorine and oxygen ions.[13,16] For the other combinations of ion–ion neutralizations, no data could be found in literature, and therefore we have adopted the same values.

Similarly, for charge transfer reactions not all rate coefficients for all ion-neutral combinations could be found in literature and therefore some data were based on comparable charge transfer reactions presented by Thorsteinsson and Gudmundsson.[13]

2.3. Surface Reactions Included in the Model

The reaction set describing the surface processes of the $SiCl_4/O_2/Ar$ plasma is presented in Table 3. Si, SiCl, SiO, and SiO_2 are non-volatile molecules or atoms, so they will stick at the surface and remain there with a high probability (~100%).[32] $SiCl_2$ and $SiCl_3$ can stick on the surface but the probabilities for these reactions are not very high. Cunge et al.[28] have deduced a sticking probability for $SiCl_2$ of 0.05 based on experimental measurements. On the other hand, $SiCl_3$ is quite reactive towards the surface. Upon impact with the wall, it can abstract Cl from the surface to form $SiCl_4$ if possible, or it can bond to the surface and remain there. Since $SiCl_3$ is near volatile like $SiCl_2$, the same value for the sticking coefficient was adopted in our simulations.

To describe the oxidation of chlorinated silicon in the model, we consider step-wise oxidation, where a chlorine atom is gradually replaced by an oxygen atom, eventually to form SiO_2. This step-wise oxidation was proposed by Cunge et al.[28] and our surface oxidation probabilities are based on this mechanism where the reactivity of O atoms is much higher than for O_2 molecules.

The chemical etching of silicon by chlorine, although included in our model, is not very likely to occur due to the high oxygen content in the plasma under study and the very low sputter yield by ions.

Finally, since there is typically no bias applied for SiO_2 coating deposition, the sputter yield is not very high and, for the conditions under study in this paper, it could be concluded that ions do not have a significant influence on the deposition process and that sputtering effects are

Plasma Process. Polym. **2013,** *10*, 714–730

DOI: 10.1002/ppap.201300005

Table 2. List of plasma reactions included in the model.

Reaction	Cross section or rate constant	Reference
1. Electron impact reactions		
$e + SiCl_4 \rightarrow SiCl_4^+ + 2e$	$\sigma(E)$	[17,18]
$e + SiCl_4 \rightarrow SiCl_3^+ + Cl + 2e$	$\sigma(E)$	[17,18]
$e + SiCl_4 \rightarrow SiCl_2^+ + Cl_2 + 2e$	$\sigma(E)$	[17,18]
$e + SiCl_4 \rightarrow SiCl^+ + Cl_2 + Cl + 2e$	$\sigma(E)$	[17,18]
$e + SiCl_4 \rightarrow Si^+ + Cl_2 + Cl_2 + 2e$	$\sigma(E)$	[17,18]
$e + SiCl_4 \rightarrow SiCl_3 + Cl^+ + 2e$	$\sigma(E)$	[17,18]
$e + SiCl_3 \rightarrow SiCl_3^+ + 2e$	$\sigma(E)$	[17,19]
$e + SiCl_3 \rightarrow SiCl_2^+ + Cl + 2e$	$\sigma(E)$	[17,19]
$e + SiCl_3 \rightarrow SiCl^+ + Cl_2 + 2e$	$\sigma(E)$	[17,19]
$e + SiCl_3 \rightarrow Si^+ + Cl_2 + Cl + 2e$	$\sigma(E)$	[17,19]
$e + SiCl_3 \rightarrow SiCl_2 + Cl^+ + 2e$	$\sigma(E)$	[17,19]
$e + SiCl_2 \rightarrow SiCl_2^+ + 2e$	$\sigma(E)$	[17,20]
$e + SiCl_2 \rightarrow SiCl^+ + Cl + 2e$	$\sigma(E)$	[17,20]
$e + SiCl_2 \rightarrow Si^+ + Cl_2 + 2e$	$\sigma(E)$	[17,20]
$e + SiCl_2 \rightarrow SiCl + Cl^+ + 2e$	$\sigma(E)$	[17,20]
$e + SiCl \rightarrow SiCl^+ + 2e$	$\sigma(E)$	[17,20]
$e + SiCl \rightarrow Si^+ + Cl + 2e$	$\sigma(E)$	[17,20]
$e + SiCl \rightarrow Si + Cl^+ + 2e$	$\sigma(E)$	[17,20]
$e + Si \rightarrow Si^+ + 2e$	$\sigma(E)$	[8]
$e + SiO \rightarrow SiO^+ + 2e$	$\sigma(E)$	[21]
$e + SiO_2 \rightarrow SiO_2^+ + 2e$	$\sigma(E)$	[21]
$e + Ar \rightarrow Ar^* + e$	$\sigma(E)$	[22]
$e + Ar \rightarrow Ar^+ + 2e$	$\sigma(E)$	[22]
$e + Ar^* \rightarrow Ar^+ + 2e$	$\sigma(E)$	[22]
$e + Ar^* \rightarrow Ar + e$	$\sigma(E)$	[22]
$e + O_2 \rightarrow O^- + O$	$\sigma(E)$	[23]
$e + O_2 \rightarrow O + O + e$	$\sigma(E)$	[23]
$e + O_2 \rightarrow O^* + O + e$	$\sigma(E)$	[23]
$e + O_2 \rightarrow O_2^+ + 2e$	$\sigma(E)$	[23]
$e + O_2 \rightarrow O + O^+ + 2e$	$\sigma(E)$	[23]
$e + O_2^+ \rightarrow O + O$	$\sigma(E)$	[23]
$e + O^- \rightarrow O + 2e$	$1.95 \times 10^{-12}\, T_e^{-0.7} \exp[-3.4\,\mathrm{eV}/T_e]\ \mathrm{cm}^3 \cdot \mathrm{s}^{-1}$	[23]
$e + O \rightarrow O^* + e$	$\sigma(E)$	[23]
$e + O \rightarrow O^+ + 2e$	$\sigma(E)$	[23]
$e + O^* \rightarrow O + e$	$\sigma(E)$	[23]
$e + O^* \rightarrow O^+ + 2e$	$\sigma(E)$	[23]
$e + Cl_2 \rightarrow Cl + Cl^-$	$\sigma(E)$	[24]
$e + Cl_2 \rightarrow Cl + Cl + e$	$\sigma(E)$	[24]
$e + Cl_2 \rightarrow Cl_2^+ + 2e$	$\sigma(E)$	[24]
$e + Cl_2^+ \rightarrow Cl + Cl$	$\sigma(E)$	[24]

(*Continued*)

Table 2. Continued

Reaction	Cross section or rate constant	Reference
$e + Cl \rightarrow Cl^* + e$	$\sigma(E)$	[24]
$e + Cl \rightarrow Cl^+ + 2e$	$\sigma(E)$	[24]
$e + Cl^* \rightarrow Cl^+ + 2e$	$\sigma(E)$	[24]
$e + Cl^- \rightarrow Cl + 2e$	$\sigma(E)$	[24]
$e + ClO \rightarrow Cl + O + e$	$1.27 \times 10^{-7}\ T_e^{-1.36}\ \exp[-6.84\,eV/T_e]\ cm^3 \cdot s^{-1}$	[13]
$e + ClO \rightarrow ClO^+ + 2e$	$9.48 \times 10^{-9}\ T_e^{0.85}\ \exp[-12.24\,eV/T_e]\ cm^3 \cdot s^{-1}$	[13]
2. Ion neutralization reactions		
$SiCl_4^+ + Cl^- \rightarrow SiCl_4 + Cl$	$10^{-7}\ [T/298\,K]^{0.5}\ cm^3 \cdot s^{-1}$	Estimated (see text)
$SiCl_4^+ + O^- \rightarrow SiCl_4 + O$	$10^{-7}\ [T/298\,K]^{0.5}\ cm^3 \cdot s^{-1}$	Estimated (see text)
$SiCl_3^+ + Cl^- \rightarrow SiCl_3 + Cl$	$10^{-7}\ [T/298\,K]^{0.5}\ cm^3 \cdot s^{-1}$	Estimated (see text)
$SiCl_3^+ + O^- \rightarrow SiCl_3 + O$	$10^{-7}\ [T/298\,K]^{0.5}\ cm^3 \cdot s^{-1}$	Estimated (see text)
$SiCl_2^+ + Cl^- \rightarrow SiCl_2 + Cl$	$10^{-7}\ [T/298\,K]^{0.5}\ cm^3 \cdot s^{-1}$	Estimated (see text)
$SiCl_2^+ + O^- \rightarrow SiCl_2 + O$	$10^{-7}\ [T/298\,K]^{0.5}\ cm^3 \cdot s^{-1}$	Estimated (see text)
$SiCl^+ + Cl^- \rightarrow SiCl + Cl$	$10^{-7}\ [T/298\,K]^{0.5}\ cm^3 \cdot s^{-1}$	Estimated (see text)
$SiCl^+ + O^- \rightarrow SiCl + O$	$10^{-7}\ [T/298\,K]^{0.5}\ cm^3 \cdot s^{-1}$	Estimated (see text)
$Si^+ + Cl^- \rightarrow Si + Cl$	$10^{-7}\ [T/298\,K]^{0.5}\ cm^3 \cdot s^{-1}$	Estimated (see text)
$Si^+ + O^- \rightarrow Si + O$	$10^{-7}\ [T/298\,K]^{0.5}\ cm^3 \cdot s^{-1}$	Estimated (see text)
$SiO^+ + Cl^- \rightarrow SiO + Cl$	$10^{-7}\ [T/298\,K]^{0.5}\ cm^3 \cdot s^{-1}$	Estimated (see text)
$SiO^+ + O^- \rightarrow SiO + O$	$10^{-7}\ [T/298\,K]^{0.5}\ cm^3 \cdot s^{-1}$	Estimated (see text)
$SiO_2^+ + Cl^- \rightarrow SiO_2 + Cl$	$10^{-7}\ [T/298\,K]^{0.5}\ cm^3 \cdot s^{-1}$	Estimated (see text)
$SiO_2^+ + O^- \rightarrow SiO_2 + O$	$10^{-7}\ [T/298\,K]^{0.5}\ cm^3 \cdot s^{-1}$	Estimated (see text)
$O^- + O_2^+ \rightarrow O + O_2$	$2.00 \times 10^{-7}\ [T/298\,K]^{-0.5}\ cm^3 \cdot s^{-1}$	[25]
$O^- + O_2^+ \rightarrow O + O + O$	$10^{-7}\ cm^3 \cdot s^{-1}$	[25]
$O^- + O^+ \rightarrow O + O$	$2.70 \times 10^{-7}\ [T/298\,K]^{-0.5}\ cm^3 \cdot s^{-1}$	[26]
$Cl^- + Cl^+ \rightarrow Cl + Cl$	$10^{-7}\ [T/298\,K]^{0.5}\ cm^3 \cdot s^{-1}$	[16]
$Cl^- + Cl_2^+ \rightarrow Cl + Cl + Cl$	$10^{-7}\ [T/298\,K]^{0.5}\ cm^3 \cdot s^{-1}$	[16]
$Cl^- + Ar^+ \rightarrow Cl + Ar$	$10^{-7}\ [T/298\,K]^{0.5}\ cm^3 \cdot s^{-1}$	[16]
$O^- + Ar^+ \rightarrow O + Ar$	$10^{-7}\ [T/298\,K]^{0.5}\ cm^3 \cdot s^{-1}$	Estimated (see text)
$O^- + Cl^+ \rightarrow O + Cl$	$5.00 \times 10^{-8}\ [T/298\,K]^{0.5}\ cm^3 \cdot s^{-1}$	Estimated from ref. [12]
$O^- + Cl_2^+ \rightarrow O + Cl_2$	$5.00 \times 10^{-8}\ [T/298\,K]^{0.5}\ cm^3 \cdot s^{-1}$	Estimated from ref. [12]
$Cl^- + O_2^+ \rightarrow Cl + O_2$	$5.00 \times 10^{-8}\ [T/298\,K]^{0.5}\ cm^3 \cdot s^{-1}$	[13]
$Cl^- + O^+ \rightarrow Cl + O$	$5.00 \times 10^{-8}\ [T/298\,K]^{0.5}\ cm^3 \cdot s^{-1}$	[13]
$Cl^- + ClO^+ \rightarrow Cl + ClO$	$5.00 \times 10^{-8}\ [T/298\,K]^{-0.5}\ cm^3 \cdot s^{-1}$	[13]
$O^- + ClO^+ \rightarrow O + ClO$	$2.60 \times 10^{-8}\ [T/298\,K]^{-0.44}\ cm^3 \cdot s^{-1}$	[13]
3. Charge transfer reactions		
$Ar^+ + Cl_2 \rightarrow Ar + Cl_2^+$	$0.84 \times 10^{-10}\ [T/298\,K]^{0.5}\ cm^3 \cdot s^{-1}$	[16]
$Ar^+ + Cl_2 \rightarrow Ar + Cl^+ + Cl$	$0.64 \times 10^{-10}\ [T/298\,K]^{0.5}\ cm^3 \cdot s^{-1}$	[16]
$Ar^+ + Cl \rightarrow Ar + Cl^+$	$2.00 \times 10^{-10}\ [T/298\,K]^{0.5}\ cm^3 \cdot s^{-1}$	[16]
$Ar^+ + O_2 \rightarrow Ar + O_2^+$	$5.10 \times 10^{-11}\ cm^3 \cdot s^{-1}$	[25]
$Ar^+ + O \rightarrow Ar + O^+$	$1.20 \times 10^{-11}\ cm^3 \cdot s^{-1}$	[25]
$O^+ + O_2 \rightarrow O + O_2^+$	$2.00 \times 10^{-11}\ cm^3 \cdot s^{-1}$	[25]

(*Continued*)

Plasma Process. Polym. **2013,** *10,* 714–730

DOI: 10.1002/ppap.201300005

Table 2. Continued

Reaction	Cross section or rate constant	Reference
$Cl^+ + Cl_2 \rightarrow Cl + Cl_2^+$	$5.40 \times 10^{-10}\ [T/298\,K]^{0.5}\ cm^3 \cdot s^{-1}$	[16]
$Cl^+ + O_2 \rightarrow Cl + O_2^+$	$4.90 \times 10^{-11}\ cm^3 \cdot s^{-1}$	Estimated (see text)
$O^+ + ClO \rightarrow O + ClO^+$	$4.90 \times 10^{-10}\ cm^3 \cdot s^{-1}$	[13]
$O_2^+ + ClO \rightarrow O_2 + ClO^+$	$4.90 \times 10^{-10}\ cm^3 \cdot s^{-1}$	[13]
$Cl^+ + ClO \rightarrow Cl + ClO^+$	$4.90 \times 10^{-10}\ cm^3 \cdot s^{-1}$	[13]
$Cl_2^+ + ClO \rightarrow Cl_2 + ClO^+$	$4.90 \times 10^{-10}\ cm^3 \cdot s^{-1}$	[13]
$Ar^+ + ClO \rightarrow Ar + ClO^+$	$4.90 \times 10^{-10}\ cm^3 \cdot s^{-1}$	Estimated (see text)
$Ar^+ + ClO \rightarrow Ar + ClO^+$	$4.90 \times 10^{-10}\ cm^3 \cdot s^{-1}$	Estimated (see text)
$O^+ + SiCl_x \rightarrow O + SiCl_x^+$	$4.90 \times 10^{-10}\ cm^3 \cdot s^{-1}$	Estimated (see text)
$O_2^+ + SiCl_x \rightarrow O_2 + SiCl_x^+$	$4.90 \times 10^{-10}\ cm^3 \cdot s^{-1}$	Estimated (see text)
$Cl^+ + SiCl_x \rightarrow Cl + SiCl_x^+$	$4.90 \times 10^{-10}\ cm^3 \cdot s^{-1}$	Estimated (see text)
$Cl_2^+ + SiCl_x \rightarrow Cl_2 + SiCl_x^+$	$4.90 \times 10^{-10}\ cm^3 \cdot s^{-1}$	Estimated (see text)
$Ar^+ + SiCl_x \rightarrow Ar + SiCl_x^+$	$4.90 \times 10^{-10}\ cm^3 \cdot s^{-1}$	Estimated (see text)
$Ar^+ + SiCl_x \rightarrow Ar + SiCl_x^+$	$4.90 \times 10^{-10}\ cm^3 \cdot s^{-1}$	Estimated (see text)
$O^+ + SiO_x \rightarrow O + SiO_x^+$	$4.90 \times 10^{-10}\ cm^3 \cdot s^{-1}$	Estimated (see text)
$O_2^+ + SiO_x \rightarrow O_2 + SiO_x^+$	$4.90 \times 10^{-10}\ cm^3 \cdot s^{-1}$	Estimated (see text)
$Cl^+ + SiO_x \rightarrow Cl + SiO_x^+$	$4.90 \times 10^{-10}\ cm^3 \cdot s^{-1}$	Estimated (see text)
$Cl_2^+ + SiO_x \rightarrow Cl_2 + SiO_x^+$	$4.90 \times 10^{-10}\ cm^3 \cdot s^{-1}$	Estimated (see text)
$Ar^+ + SiO_x \rightarrow Ar + SiO_x^+$	$4.90 \times 10^{-10}\ cm^3 \cdot s^{-1}$	Estimated (see text)
4. Other chemical reactions between neutral heavy particles		
$Si + Cl_2 \rightarrow SiCl + Cl$	$3.30 \times 10^{-10}\ cm^3 \cdot s^{-1}$	[27]
$SiCl + Cl_2 \rightarrow SiCl_2 + Cl$	$5.30 \times 10^{-11}\ cm^3 \cdot s^{-1}$	[28]
$Si + O_2 \rightarrow SiO + O^*$	$1.73 \times 10^{-10}\ [T/298\,K] - 0.53\ \exp[-17\,K/T]\ cm^3 \cdot s^{-1}$	[29,30]
$SiO + O_2 \rightarrow SiO_2 + O$	$2.36 \times 10^{-10}\ \exp[-3266.3\,K/T]\ cm^3 \cdot s^{-1}$	[30,31]
$O^* + O \rightarrow O + O$	$8.00 \times 10^{-12}\ cm^3 \cdot s^{-1}$	[25]
$O^* + O_2 \rightarrow O + O_2$	$2.65 \times 10^{-11}\ \exp[67\,K/T]\ cm^3 \cdot s^{-1}$	[25]
$Cl_2 + O^* \rightarrow ClO + Cl$	$2.11 \times 10^{-10}\ cm^3\,s^{-1}$	[13]
$ClO + O \rightarrow O_2 + Cl$	$4.11 \times 10^{-11}\ \exp[42\,K/T]\ cm^3 \cdot s^{-1}$	[13]
$Ar^* + Cl_2 \rightarrow Ar + Cl_2^+ + e$	$7.10 \times 10^{-10}\ [T/298\,K]^{0.5}\ cm^3 \cdot s^{-1}$	[16]
$Ar^* + Cl \rightarrow Ar + Cl^*$	$0.70 \times 10^{-11}\ [T/298\,K]^{0.5}\ cm^3 \cdot s^{-1}$	[16]
$Ar^* + Ar^* \rightarrow Ar^+ + Ar + e$	$5.00 \times 10^{-10}\ cm^3 \cdot s^{-1}$	[16]

negligible (i.e., below threshold). However, some ions can also account for deposition and these probabilities are taken the same as those of their neutral equivalents, which is the case for $SiCl_3^+$, $SiCl_2^+$, $SiCl^+$, Si^+, SiO^+, and SiO_2^+.

3. Experimental

The SiO_2 layers are deposited in a 300 mm LAM Research ICP 2300 Versys Kiyo 3X etch reactor. Prior to deposition, the native SiO_2 layer is removed from the wafers with an HF(49%)/O_3 dip. The deposited SiO_2 thickness after plasma processing is determined by means of a SCD100 spectroscopic ellipsometer (235–750 nm) from KLA Tencor. A two-layer model is used for analysis. The first layer is the Si substrate itself with fixed optical parameters. The second layer is the deposited SiO_2, which is described by a harmonic oscillator model. The goodness-of-fit for the results presented in this paper is between 0.7 and 0.9.

Table 3. Overview of the surface reactions included in the model.

Surface reaction	Probability	Reference
1. Deposition of low- or non-volatile products		
$Si + surface \rightarrow Si_{(s)} + surface$	1.00	[32]
$SiCl + surface \rightarrow SiCl_{(s)} + surface$	1.00	[32]
$SiCl_2 + surface \rightarrow SiCl_{2(s)} + surface$	0.05[a]	[28]
$SiCl_3 + surface \rightarrow SiCl_{3(s)} + surface$	0.05[a]	[28]
$SiCl_4 + surface \rightarrow SiCl_4 + surface$	1.00	[32]
$SiO + surface \rightarrow SiO_{(s)} + surface$	1.00	[32]
$SiO_2 + surface \rightarrow SiO_{2(s)} + surface$	1.00	[32]
2. Oxidation of the surface		
$O + SiCl_{x(s)} \rightarrow SiCl_xO_{(s)}$ $(x = 0 - 3)$	1.00	Based on ref. [28]
$O + SiCl_xO_{(s)} \rightarrow SiCl_{x-1}O_{(s)} + Cl$ $(+O)$ $(x = 1 - 3)$	1.00[b]	Based on ref. [28]
$O + SiO_{(s)} \rightarrow SiO_{2(s)}$	1.00	Based on ref. [28]
$O + SiO_{2(s)} \rightarrow SiO_{2(s)} + O$	1.00	Based on ref. [28]
$O_2 + SiCl_{x(s)} \rightarrow SiCl_xO_{(s)} + O$ $(x = 0 - 3)$	0.01	Based on ref. [28]
$O_2 + SiCl_xO_{(s)} \rightarrow SiCl_{x-1}O_{(s)} + Cl$ $(+O_2)$ $(x = 1 - 3)$	0.01[b]	Based on ref. [28]
$O_2 + SiO_{(s)} \rightarrow SiO_{2(s)} + O$	0.01	Based on ref. [28]
$O_2 + SiO_{2(s)} \rightarrow SiO_{2(s)} + O_2$	1.00	Based on ref. [28]
$ClO + SiCl_{x(s)} \rightarrow SiCl_{x+1}O_{(s)}$ $(x = 0 - 2)$	1.00	Based on ref. [28]
$ClO + SiCl_{3(s)} \rightarrow SiCl_3O_{(s)} + Cl$	1.00	Based on ref. [28]
$ClO + SiCl_xO_{(s)} \rightarrow SiCl_{x-1}O_{(s)} + 2\ Cl$ $(+O)$ $(x = 1 - 3)$	1.00[b]	Based on ref. [28]
$ClO + SiO_{(s)} \rightarrow SiO_{2(s)} + Cl$	1.00	Based on ref. [28]
$ClO + SiO_{2(s)} \rightarrow SiO_{2(s)} + ClO$	1.00	Based on ref. [28]
3. Chlorination of the surface, leading to etching		
$Cl + Si_{(s)} \rightarrow SiCl_{(s)}$	1.00	[33]
$Cl + SiCl_{(s)} \rightarrow SiCl_{2(s)}$	0.20	[33]
$Cl + SiCl_{2(s)} \rightarrow SiCl_{3(s)}$	0.15	[33]
$Cl + SiCl_{3(s)} \rightarrow SiCl_4$	0.001	[33]
$Cl_2 + Si_{(s)} \rightarrow SiCl_{2(s)}$	0.01	[33]
$Cl_2 + SiCl_{(s)} \rightarrow SiCl_{2(s)} + Cl$	0.01	[33]
$Cl_2 + SiCl_{2(s)} \rightarrow SiCl_{3(s)} + Cl$	0.01	[33]
$Cl_2 + SiCl_{3(s)} \rightarrow SiCl_4 + Cl$	0.0001	[33]

[a]The wall loss probability for $SiCl_2$ was taken from Cunge et al.,[28] and the same value is adopted for $SiCl_3$. [b]The remaining O atom or O_2 molecule will diffuse into the layer in our model and does not return to the plasma.

4. Results and Discussion

4.1. General Plasma Properties

The two-dimensional half cross section of the ICP reactor under study is shown in Figure 1.[34] When rotating this plane around the left axis, the full cylindrical reactor is obtained. The gas is pumped into the chamber by the nozzle, which is located in the center of the top window.

Calculations are performed for the following operating conditions: 13.56 MHz coil operating frequency, 10 mTorr chamber pressure, 1 200 W coil power, 60 °C wall and substrate temperature, 120 °C dielectric window temperature, 30 sccm $SiCl_4$, 60 sccm O_2, 310 sccm Ar gas flow rate, and 44 s operating time.

a. Importance of the various plasma species

The calculated volume averaged densities of all species are listed in Table 4, sorted from highest to lowest density, including their main production and loss processes. Ar is by

Plasma Process. Polym. **2013,** *10*, 714–730

DOI: 10.1002/ppap.201300005

far the dominant species in the discharge, with a density of more than a factor 20 higher than the O_2 density and almost two orders of magnitude higher than the $SiCl_4$ density. Ar atoms can only be lost by electron impact excitation and ionization, whereas the molecular gases can also be converted into radicals and atoms, by dissociation, dissociative ionization and/or dissociative attachment. The latter processes are very important, as is demonstrated by the high densities of Cl and O atoms, which are signficantly higher than their parent gas molecules. The Cl and O atoms are indeed mainly formed by electron impact dissociative ionization of $SiCl_4$ and by electron impact dissociative attachment of O_2, respectively, as appears from Table 4. Other important plasma species are $SiCl_3$ and $SiCl_2$, with a density only a factor of 2–3 lower than the $SiCl_4$ density, making them the most important deposition precursors in spite of their much lower deposition probability (i.e., 0.05 for $SiCl_{2-3}$ versus 1.00 for the other species; see Table 3).

Concerning the ions, the most abundant positive ion in the plasma is Cl^+, closely followed by $SiCl_3^+$ and it is interesting to note that the Ar^+ density is much lower. Indeed, in the case of $SiCl_4$ and the $SiCl_x$ radicals, dissociative ionization is almost equally important as direct ionization resulting in a high total production of Cl^+ ions, whereas Ar^+ can only be formed from electron impact ionization of Ar.

Another important production process for Cl^+ ions is direct ionization of Cl atoms, which have a high abundancy in the plasma as their density can build up to higher values than the $SiCl_x$ densities. The ionization potentials of Ar and Cl are 15.76 and 12.99 eV, respectively and Cl is therefore more easily ionized. Nevertheless, the largest single production process for electrons is still direct ionization of Ar, as mentioned in Table 4.

For all positive ions, wall neutralization is found to be by far the most important loss process (i.e., $\sim 4 \times 10^{19}\,s^{-1}$). On the other hand, the negative ions are mainly lost by cation–anion neutralization, as they cannot easily reach the reactor walls.

b. Behavior of the deposition precursors in the plasma

The most important precursors for deposition are the non-volatile dissociation products of $SiCl_4$, i.e., $SiCl_3$, $SiCl_2$, and SiCl. Si, SiO, and SiO_2 will only have a minor contribution to film growth due to their much lower densities in the plasma as is clear from Table 4. The density profiles of $SiCl_4$ and of the most abundant deposition precursors are plotted in Figure 2a–d.

Comparing these density profiles indicates a stepwise dissociation process from $SiCl_4$ towards SiCl in the bulk plasma. Indeed, it is more likely to create $SiCl_3$ from $SiCl_4$, $SiCl_2$ from $SiCl_3$ and so on, abstracting only one Cl atom or Cl^+ ion each time.[17,18] This explains the maxima of the densities of $SiCl_{1-3}$ since the gas is injected towards the center of the wafer and then disperses in the lateral direction. Indeed, the maximum densities of the "higher-stage dissociation products" tend to be more or less located gradually further away from the nozzle. The calculated densities of the various $SiCl_x$ species are in qualitative agreement with several experimental papers on the plasma-induced fragmentation of $SiCl_4$ into $SiCl_x$ species. It is generally found that the most abundant dissociation product is $SiCl_3$, followed by $SiCl_2$ and SiCl.[35–40] Furthermore, of all $SiCl_4$ molecules entering the plasma reactor, 32% is finally lost at the walls for growing the coating.

It is also apparent from Figure 2b that $SiCl_3$ has a small local second maximum underneath the top window next to the nozzle, which can be explained by a fraction of the flow of $SiCl_4$ that dissipates horizontally near the top window besides the stronger vertically directed jet-like flow towards the center of the wafer. It was confirmed that this small local maximum near the top window was not a numerical artifact as it covers a few layers of computational cells.

The gradual dissociation of $SiCl_4$ into $SiCl_3$, $SiCl_2$, SiCl, and eventually Si entails the creation of a large number of Cl atoms. Since Cl atoms have a very low wall loss probability on a SiO_2 coating its density can build up significantly during plasma coating growth (see Table 4).[41]

c. Behavior of the oxidizing agents in the plasma

The deposited $SiCl_x$ layers must be oxidized towards the formation of a SiO_2 coating. For this, the fraction of oxidizing species in the gas mixture is typically chosen to be at least twice that of $SiCl_4$ to assure proper/complete oxidation.

As mentioned earlier, oxidation in the bulk plasma and subsequent deposition of SiO_{1-2} is not likely, as it is reported that $SiCl_x$ molecules will only be oxidized in the gas phase at a gas temperature of at least 1 500 K, which is much higher than the calculated gas temperature under these conditions (<600 K).[15]

The most important oxidizing agents are O and O_2. Both have comparable volume averaged densities (see Table 4) but it is generally known that O atoms are more reactive. Despite their high reactivity, the overall calculated wall loss probability for O atoms was found to be very small, i.e., 0.03. There are more than sufficient O atoms present in the plasma to make certain that the coating is practically always consisting of SiO_2 during growth. Since the fluxes of the deposition precursors are at least one order of magnitude lower compared to the O and O_2 fluxes and since $SiCl_3$ and $SiCl_2$ have low sticking probabilities, oxidation of the film occurs much faster than its growth. O can also be lost at the SiO_2-like walls by recombination to O_2, but the probability of this process is expected to be low as well. Indeed, Takeshi and Lieberman reported that the recombination coefficient for O atoms should be in the order of

Table 4. List of the plasma species included in the model, sorted by magnitude of their volume-averaged densities, including their most important production and loss processes, as obtained from the model.

Species	Density (cm^{-3})	Leading production process	Leading loss process
Ar	1.75×10^{14}	Gas inlet	$e + Ar \rightarrow Ar^* + e$
Cl	2.80×10^{13}	$e + SiCl_4 \rightarrow SiCl_3^+ + Cl + 2e$	$e + Cl \rightarrow Cl^* + e$
O	9.41×10^{12}	$e + O_2 \rightarrow O^- + O$	$e + O \rightarrow O^* + e$
O_2	7.67×10^{12}	Gas inlet	$e + O_2 \rightarrow O^- + O$
$SiCl_4$	2.18×10^{12}	Gas inlet	$e + SiCl_4 \rightarrow SiCl_4^+ + 2e$
$SiCl_3$	1.17×10^{12}	$e + SiCl_4 \rightarrow SiCl_3 + Cl^+ + 2e$	$e + SiCl_3 \rightarrow SiCl_3^+ + 2e$
$SiCl_2$	8.15×10^{11}	$e + SiCl_3 \rightarrow SiCl_2 + Cl^+ + 2e$	$e + SiCl_2 \rightarrow SiCl_2^+ + 2e$
O^*	5.90×10^{11}	$e + O \rightarrow O^* + e$	$O^* + wall \rightarrow O + wall$
Cl^*	2.29×10^{11}	$e + Cl \rightarrow Cl^* + e$	$e + Cl^* \rightarrow Cl^+ + 2e$
Electrons (e)	7.66×10^{10}	$e + Ar \rightarrow Ar^+ + 2e$	$e + wall \rightarrow wall$
Cl^+	3.89×10^{10}	$e + Cl \rightarrow Cl^+ + 2e$	$Cl^+ + wall \rightarrow Cl + wall$
SiCl	2.64×10^{10}	$e + SiCl_2 \rightarrow SiCl + Cl^+ + 2e$	$SiCl + wall \rightarrow SiCl_{(s)} + wall$
$SiCl_3^+$	2.08×10^{10}	$e + SiCl_4 \rightarrow SiCl_3^+ + Cl + 2e$	$SiCl_3^+ + wall \rightarrow SiCl_3 + wall$
$SiCl^+$	7.63×10^{9}	$e + SiCl_2 \rightarrow SiCl^+ + Cl + 2e$	$SiCl^+ + wall \rightarrow SiCl + wall$
Ar^*	6.28×10^{9}	$e + Ar \rightarrow Ar^* + e$	$e + Ar^* \rightarrow Ar^+ + 2e$
$SiCl_4^+$	5.75×10^{9}	$e + SiCl_4 \rightarrow SiCl_4^+ + 2e$	$SiCl_4^+ + wall \rightarrow SiCl_4 + wall$
$SiCl_2^+$	3.01×10^{9}	$e + SiCl_3 \rightarrow SiCl_2^+ + Cl + 2e$	$SiCl_2^+ + wall \rightarrow SiCl_2 + wall$
Ar^+	1.79×10^{9}	$e + Ar \rightarrow Ar^+ + 2e$	$Ar^+ + wall \rightarrow Ar + wall$
O^-	1.78×10^{9}	$e + O_2 \rightarrow O^- + O$	$O^- + Cl^+ \rightarrow O + Cl$
Si	1.30×10^{9}	$e + SiCl \rightarrow Si + Cl^+ + 2e$	$e + Si \rightarrow Si^+ + 2e$
SiO	1.24×10^{9}	$Si + O_2 \rightarrow SiO + O^*$	$SiO + wall \rightarrow SiO_{(s)} + wall$
Cl_2	5.61×10^{8}	$e + SiCl_4 \rightarrow SiCl_2^+ + Cl_2 + 2e$	$e + Cl_2 \rightarrow Cl_2^+ + 2e$
O_2^+	2.71×10^{8}	$e + O_2 \rightarrow O_2^+ + 2e$	$O_2^+ + wall \rightarrow O_2 + wall$
Si^+	1.64×10^{8}	$e + SiCl \rightarrow Si^+ + Cl + 2e$	$Si^+ + wall \rightarrow Si + wall$
O^+	8.68×10^{7}	$e + O \rightarrow O^+ + 2e$	$O^+ + wall \rightarrow O + wall$
Cl^-	4.20×10^{7}	$e + Cl_2 \rightarrow Cl + Cl^-$	$SiCl_3^+ + Cl^- \rightarrow SiCl_3 + Cl$
ClO	1.26×10^{7}	$Cl_2 + O^* \rightarrow ClO + Cl$	$e + ClO \rightarrow Cl + O + e$
SiO_2	2.55×10^{6}	$SiO + O_2 \rightarrow SiO_2 + O$	$SiO_2 + wall \rightarrow SiO_{2(s)} + wall$
ClO^+	2.26×10^{6}	$e + ClO \rightarrow ClO^+ + 2e$	$ClO^+ + wall \rightarrow ClO + wall$
SiO^+	5.67×10^{5}	$e + SiO \rightarrow SiO^+ + 2e$	$SiO^+ + wall \rightarrow SiO + wall$
Cl_2^+	1.95×10^{5}	$e + Cl_2 \rightarrow Cl_2^+ + 2e$	$Cl_2^+ + wall \rightarrow Cl_2 + wall$
SiO_2^+	8.22×10^{3}	$e + SiO_2 \rightarrow SiO_2^+ + 2e$	$SiO_2^+ + wall \rightarrow SiO_2 + wall$

A species with a (s)-subscript denotes a surface species.

0.0001 on a glass surface in a pressure range of 1–100 mTorr.[41]

4.2. General Properties of the Coating

The calculated chemical composition of the coating on the various reactor surfaces, for the same conditions as mentioned in the beginning of the results and discussion section, is presented in Figure 3.

It is clear that for a 2:1 O_2:$SiCl_4$ ratio the chemical composition is very uniform and very close to stoichiometric SiO_2 on all surfaces. The amount of chlorine trapped in the layer is very low (~1%) with a maximum of about 3% in the center of the wafer and near the gas nozzle. The slight increase in chlorine content in these locations is due to a local higher deposition rate, resulting in a thicker coating which is shown in Figure 4, and the latter is in turn

Plasma Process. Polym. **2013,** *10*, 714–730

DOI: 10.1002/ppap.201300005

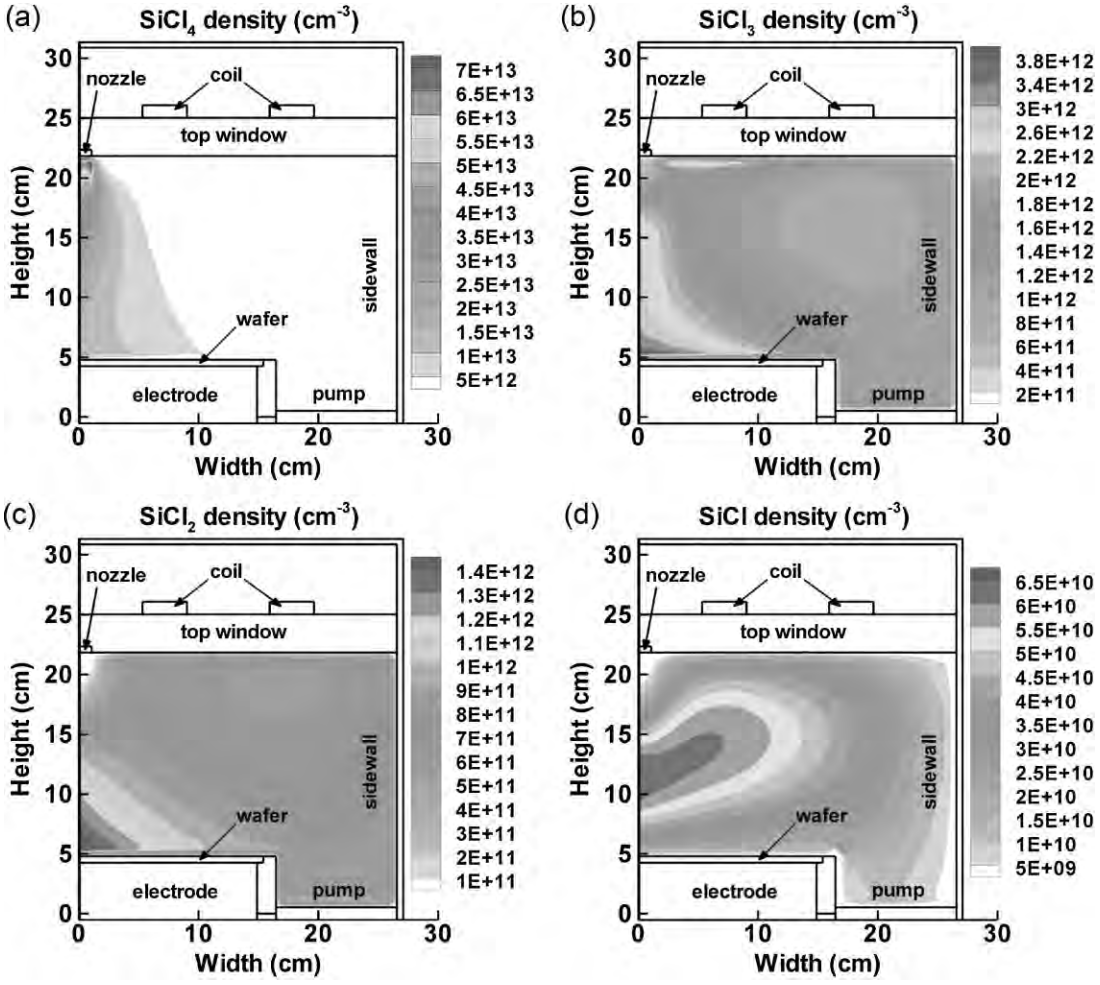

Figure 2. Calculated two-dimensional density profiles of (a) $SiCl_4$, (b) $SiCl_3$, (c) $SiCl_2$, and (d) SiCl, for the conditions mentioned in the beginning of the results and discussion section.

attributed to a higher flux of $SiCl_x$ species, as shown in Figure 5. Since the layer is efficiently oxidized towards SiO_2 during growth, the chemical etching rate by chlorine radicals was found to be negligible, i.e., three orders of magnitude lower than the total deposition rate.

The thickness of the coating is not very uniform, ranging from 20–50 nm at the sidewall to maxima of 300 nm at the center of the wafer and 420 nm at the top window near the gas inlet and the calculated coating thickness on the wafer surface is in good agreement with the measured values. The small peak at around 17 cm is a numerical artifact (i.e., a corner effect) when moving from the horizontal surface of the confinement ring to its vertical surface (see Figure 1).

The thickness uniformity is directly dependent on the flux uniformity of the deposition precursors. These species have higher fluxes at the center of the wafer and near the nozzle, as is clear from Figure 5, which are, in turn dependent on their bulk plasma density uniformities as shown in Figure 2b–d. As mentioned before, a sufficiently high oxygen flux is necessary to ensure complete oxidation of the $SiCl_xO$ film into SiO_2. It is therefore expected that a higher deposition rate will result in more trapping of chlorine during the film formation.

The $SiCl_3$, $SiCl_2$, and SiCl species each contribute for about 47, 32, and 13% to the film growth, respectively. The remaining 8% is deposited by less abundant species such as $SiCl_3^+$, $SiCl_2^+$, and Si.

We can conclude that the chemical composition of the coating is already close to SiO_2 at all reactor walls, but the coating thickness is not very uniform, which can be explained from the fluxes of the $SiCl_x$ growth precursors towards the walls. Moreover, the thickness non-uniformity is more pronounced compared to the flux non-uniformity due to the fact that the deposited layer is highly porous. In order to find out whether this uniformity can be improved, we will investigate in the following sections the effect

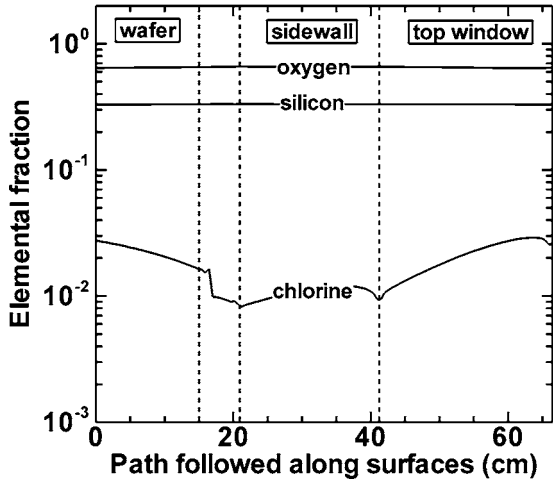

Figure 3. Calculated chemical composition of the deposited coating on the wafer, sidewall and top window, for the same conditions as mentioned in the beginning of the results and discussion section. The *x*-axis corresponds to the dashed arrow path illustrated in Figure 1.

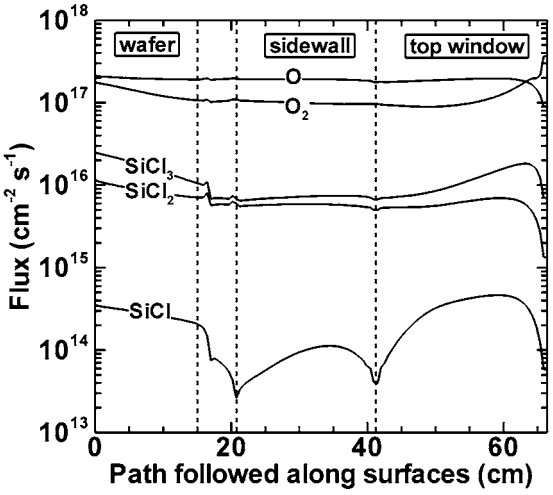

Figure 5. Calculated fluxes of O, O_2, $SiCl_3$, $SiCl_2$, and SiCl towards the wafer, sidewall and top window, for the same conditions as mentioned in the beginning of the results and discussion section. The *x*-axis corresponds to the dashed arrow path illustrated in Figure 1.

of varying the operating conditions, such as gas flow, operating power, and gas pressure.

4.3. Effect of Gas Flow

Figure 6 presents the calculated coating thickness at a total gas flow of 100 and 400 sccm, keeping all other operating conditions, including the Ar:$SiCl_4$:O_2 gas ratio, the same as mentioned in the beginning of the results and discussion section. Moreover, also the measured coating thickness at the wafer surface is indicated for both gas flow values, and very good agreement is reached with the calculation results. A lower gas flow means less supply of $SiCl_4$ molecules in the reactor within a fixed time and hence a lower source of $SiCl_x$ species, so it is expected to result in a thinner film in general. However, it cannot simply be said

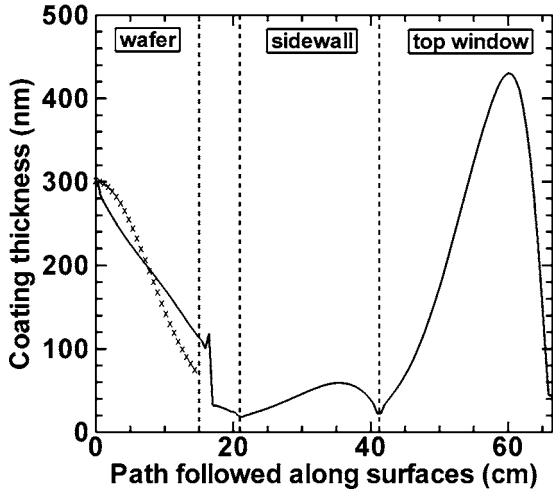

Figure 4. Calculated thickness of the deposited coating on the wafer, sidewall and top window after 44 s of processing time, for the same conditions as mentioned in the beginning of the results and discussion section. The *x*-axis corresponds to the dashed arrow path illustrated in Figure 1. The x-shaped datapoints represent the experimentally measured coating thickness on the wafer.

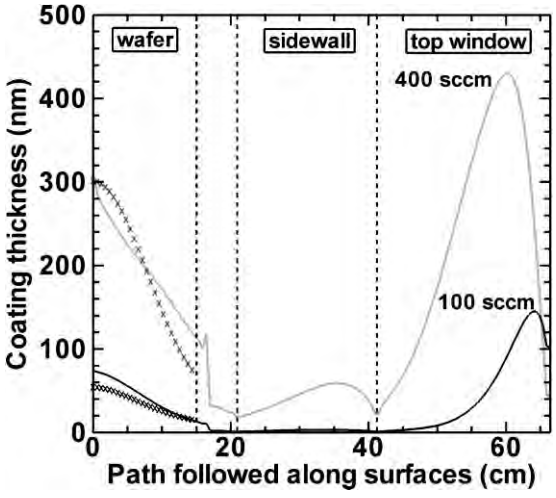

Figure 6. Calculated coating thickness for a total gas flow of 100 sccm (black curve) and 400 sccm (grey curve). The other operating conditions are the same as in the beginning of the results and discussion section. The *x*-axis corresponds to the dashed arrow path illustrated in Figure 1. The x-shaped datapoints represent the experimentally measured coating thickness on the wafer, again in black for the 100 sccm case and in gray for the 400 sccm case.

Plasma Process. Polym. **2013,** *10*, 714–730

DOI: 10.1002/ppap.201300005

that the deposition rate will be four times lower according to this different gas flow, as still the same amount of molecules are present in the reactor since the pumping speed is adjusted to maintain a fixed pressure of 10 mTorr. At 400 sccm gas flow, the residence time of the species in the reactor, as calculated in our model, is 0.09 s, whereas at 100 sccm it was found to be (naturally) about four times longer at the same chamber pressure of 10 mTorr. A longer residence time entails a higher dissociation degree of $SiCl_4$ into $SiCl_x$ products, even if the operating power is the same, as $SiCl_4$ has more time to be dissociatied before being pumped out. Indeed, at 100 sccm, $SiCl_4$ is dissociated for 68%, which is clearly higher than the dissociation degree at 400 sccm (i.e., 52%). In spite of this higher dissociation degree, the volume averaged plasma densities of all $SiCl_{1-3}$ species are found to be roughly five times lower at 100 sccm than at 400 sccm, because these species still become lost at the walls with the same probability. Hence, as the source function of the $SiCl_x$ species (i.e., the $SiCl_4$ supply) is reduced by the lower gas flow, and the most important loss function is the same (i.e., wall loss), the balanced densities in the bulk plasma and therefore also the fluxes of $SiCl_{1-3}$ are smaller at a lower gas flow, which results in a lower deposition rate and hence coating thickness, as indeed shown in Figure 6.

The volume-averaged densities of $SiCl_{1-4}$, O, and O_2 for both conditions are shown in Table 5. The densities at 200 W operating power and 60 mTorr pressure are listed as well, since they will be discussed in the following sections.

The relative contributions of $SiCl_3$ and $SiCl_2$ species to the film growth are found to be higher at 100 sccm than at 400 sccm (i.e., 53 and 45% for $SiCl_3$ and $SiCl_2$ at 100 sccm, vs. 47 and 32% at 400 sccm), whereas the contribution of SiCl is lower (i.e., 1% at 100 sccm, vs. 13% at 400 sccm). These relative contributions are strongly correlated to the ratio of their volume-averaged densities, as listed in Table 5.

The density profiles of the most important precursors (i.e., $SiCl_3$, $SiCl_2$, and SiCl) at 100 sccm gas flow are found to be very similar to those already presented in Figure 2a–d for 400 sccm, except that the maximum densities are located closer towards the nozzle, as the gases (and the $SiCl_x$ species) move more slowly in the reactor volume due to the lower gas flow rate.

Finally, the chemical composition of the coating also appears to be very similar ($\sim SiO_2$) for 100 and 400 sccm. It is expected that the chemical composition can be directly altered by tuning the $SiCl_4/O_2$ gas ratio. The effect of oxygen flow on the chemical state of the SiO_2 layer created by PECVD was already investigated by Ortiz et al.[7]

It can be concluded that a variation of the gas flow allows control of the film thickness at a fixed pressure and power without significantly improving the thickness uniformity or chemical composition for the conditions under study here.

4.4. Effect of Operating Power

The calculated coating thicknesses, for an operating power of 200 and 1 200 W, keeping all other conditions the same, are illustrated in Figure 7, together with the measured coating thickness at the wafer surface. The dissociation degree of $SiCl_4$ is calculated to be only 14% at 200 W, compared to 52% at 1 200 W. Furthermore, the density of $SiCl_3$ is also slightly higher at 200 W, but the next-stage dissociation products (i.e., $SiCl_2$ and SiCl) have significantly lower densities (see Table 5). These higher-stage dissociation products are indeed not likely created in the plasma at lower power. The density of $SiCl_3$, on the other hand, seems to be less influenced by power, as its production rate is based on dissociation of $SiCl_4$ and its loss rate is based on further dissociation towards the formation of $SiCl_2$ or SiCl. Hence, both production and loss

Table 5. Volume averaged densities of the most relevant species responsible for coating growth, listed at different operating conditions for comparison.

Species	Standard conditions (cm^{-3})	100 sccm	200 W	60 mTorr
$SiCl_4$	1.89×10^{12}	$1.84 \times 10^{11}\ cm^{-3}$	$1.33 \times 10^{13}\ cm^{-3}$	$2.15 \times 10^{13}\ cm^{-3}$
$SiCl_3$	1.05×10^{12}	$2.46 \times 10^{11}\ cm^{-3}$	$1.62 \times 10^{12}\ cm^{-3}$	$3.00 \times 10^{12}\ cm^{-3}$
$SiCl_2$	7.17×10^{11}	$1.59 \times 10^{11}\ cm^{-3}$	$3.39 \times 10^{11}\ cm^{-3}$	$2.34 \times 10^{12}\ cm^{-3}$
SiCl	2.52×10^{10}	$6.90 \times 10^{9}\ cm^{-3}$	$1.25 \times 10^{9}\ cm^{-3}$	$8.81 \times 10^{10}\ cm^{-3}$
O	1.07×10^{13}	$5.98 \times 10^{12}\ cm^{-3}$	$1.27 \times 10^{12}\ cm^{-3}$	$8.06 \times 10^{11}\ cm^{-3}$
O_2	6.60×10^{12}	$1.84 \times 10^{12}\ cm^{-3}$	$2.99 \times 10^{13}\ cm^{-3}$	$1.13 \times 10^{14}\ cm^{-3}$

The standard conditions are mentioned in the beginning of the results and discussion section.

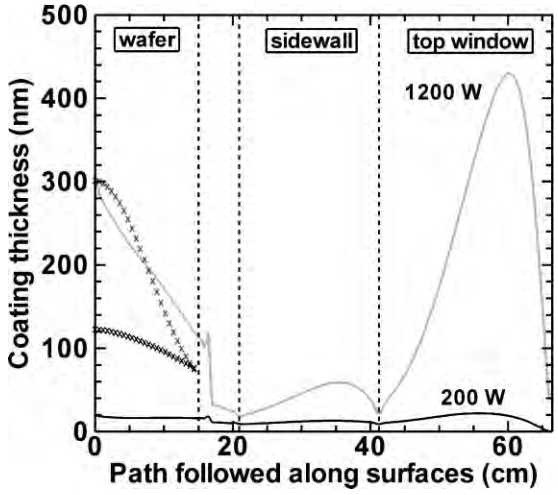

Figure 7. Calculated coating thickness at 1 200 W (gray curve) and 200 W (black curve) operating power. The other operating conditions are the same as in the beginning of the results and discussion section. The *x*-axis corresponds to the dashed arrow path illustrated in Figure 1. The x-shaped datapoints represent the experimentally measured coating thickness on the wafer, again in gray for the 1 200 W case and in black for the 200 W case.

terms are reduced at lower power, and they seem to be balanced particularly for $SiCl_3$. As the overall density of the depositing species is lower, this results in a lower film growth rate explaining the reduced coating thickness, displayed in Figure 7.

Our model predicts that the coating becomes thinner and significantly more uniform at lower power due to the lower dissociation degree of $SiCl_4$ in the plasma. However, the comparison with the measured thickness on the wafer illustrates that the calculated thickness is underestimated by the model. This will be explained in more detail in the following section.

The density profiles of $SiCl_4$, $SiCl_3$, $SiCl_2$, and SiCl at the operating power of 200 W are shown in Figure 8a–d. The plasma is more uniform at this lower power, with especially less prounounced peaks in the $SiCl_3$ and $SiCl_2$ density profiles near the wafer and nozzle, what gives rise to more uniform fluxes along the reactor surfaces.

The fluxes of the relevant species for coating formation on the different reactor surfaces are presented in Figure 9 for 200 and 1 200 W operating powers.

The $SiCl_3$ and $SiCl_2$ fluxes are indeed much more uniform at 200 than at 1 200 W. The SiCl flux, on the other hand, seems to be equally non-uniform at both power values, but its contribution to the silicon chloride film growth has dropped significantly at 200 W, to about 0.03% compared to 13% at 1 200 W.

Furthermore, at 200 W the O_2 flux is about an order of magnitude higher than the O flux, which is significantly different compared to the case at 1 200 W. Due to the much lower flux of atomic oxygen arriving at the walls, the oxidation of the deposited layer is more modest at lower power, which results in a higher concentration of trapped chlorine in the film during growth. Indeed, as illustrated in Figure 10, the SiO_2 film contains ~7% undesired chlorine at 200 W coil power, compared to only 1–3% at 1 200 W.

4.5. Effect of Gas Pressure

In Figure 11, the coating thickness is plotted for chamber pressures of 10 and 60 mTorr, keeping the other operating conditions the same. Experimentally we found that at 60 mTorr, the coating is thicker and less uniform on the wafer compared to the 10 mTorr case, but the model predicts the opposite. This underestimation of the coating thickness by the model is explained as follows: In the experiments, the nozzle is a very small needle-like tube, injecting the gas at very high speed towards the center of the wafer. In the model, the smallest size the nozzle can have is one computational cell, which is in this case about 0.5 cm wide. Since an identical gas flow is defined for both experiment and model (i.e., 400 sccm), the actual speed of the species when they are launched towards the wafer is therefore underestimated in the model. Hence, while the model can predict the coating thickness properly under most other conditions (see previous sections), it seems to underestimate the coating thickness at lower power and higher pressure. Indeed, these conditions result in a lower flux of $SiCl_3$ and $SiCl_2$ towards the wafer. Note, however, that this effect is very local and only applies to the wafer. Indeed, while the species are launched towards the wafer in a strong laminar flow, the arrival of deposition precursors on the sidewall and top window is much more dependent on diffusion within the reactor volume. It is therefore expected that the calculated coating thickness on sidewall and top window are closer to reality compared to the prediction on the wafer and the model therefore can still provide us with useful information.

As the diffusion coefficients of the plasma species in the reactor are inversely proportional to the gas pressure, the species will diffuse more slowly within the reactor volume at higher pressure, which generally yields more uniform fluxes along the reactor surfaces. Therefore, as also predicted by the model, we expect the coating thickness to be slightly more uniform on the reactor surfaces, except for the wafer due to the local vertical "nozzle jet-flow effect" which results in an even worse uniformity specifically in this location, as illustrated by the experimental results in Figure 11.

The fluxes of the species important for coating growth at 60 mTorr are presented in Figure 12. While we now know that the calculated fluxes towards the wafer are

Plasma Process. Polym. **2013,** *10*, 714–730

DOI: 10.1002/ppap.201300005

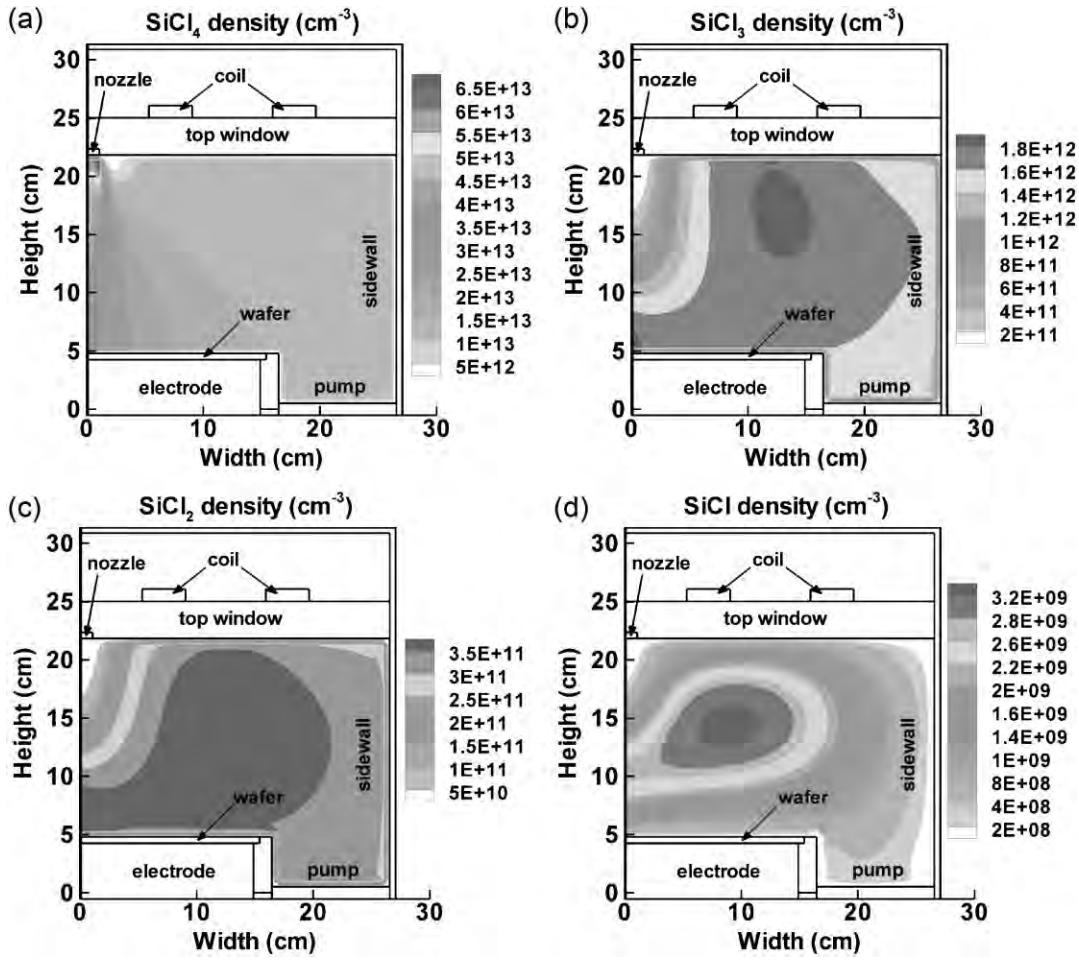

Figure 8. Calculated two-dimensional density profiles of (a) $SiCl_4$, (b) $SiCl_3$, (c) $SiCl_2$, and (d) SiCl at 200 W. The other operating conditions are the same as in the beginning of the results and discussion section.

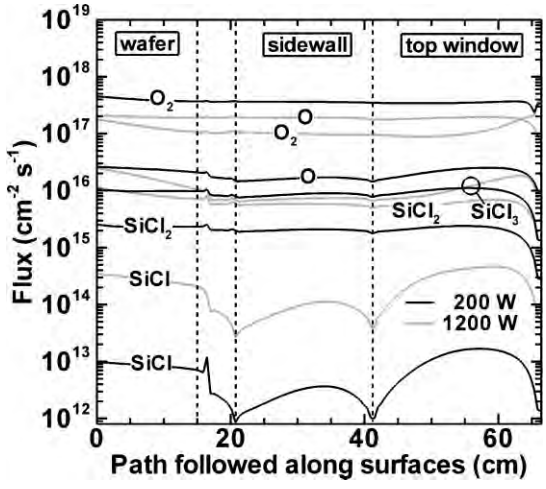

Figure 9. Calculated fluxes of the relevant neutral species for SiO_2 film deposition at 200 and 1200 W operating powers. The other operating conditions are the same as in the beginning of the results and discussion section. The *x*-axis corresponds to the dashed arrow path illustrated in Figure 1.

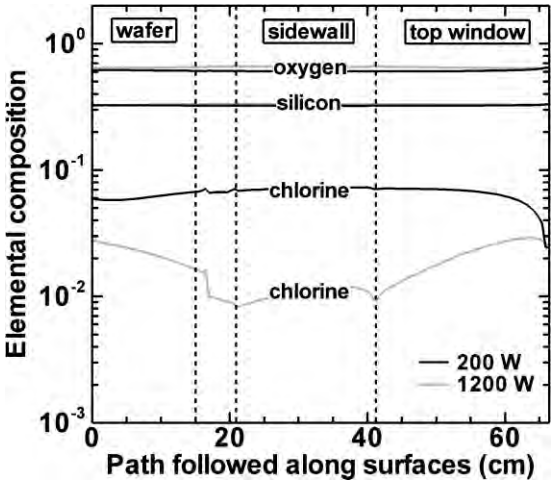

Figure 10. Calculated chemical composition of the deposited coating for 1200 and 200 W coil power. The other operating conditions are the same as in the beginning of the results and discussion section. The *x*-axis corresponds to the dashed arrow path illustrated in Figure 1.

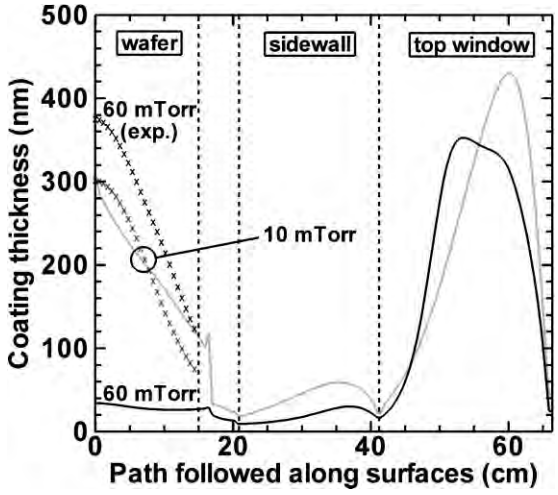

Figure 11. Calculated coating thickness at 10 mTorr (gray curve) and 60 mTorr (black curve) chamber pressure. The other operating conditions are the same as in the beginning of the results and discussion section. The x-shaped datapoints represent the experimentally measured coating thickness on the wafer, again in gray for the 10 mTorr case and in black for the 60 mTorr case. The *x*-axis corresponds to the dashed arrow path illustrated in Figure 1.

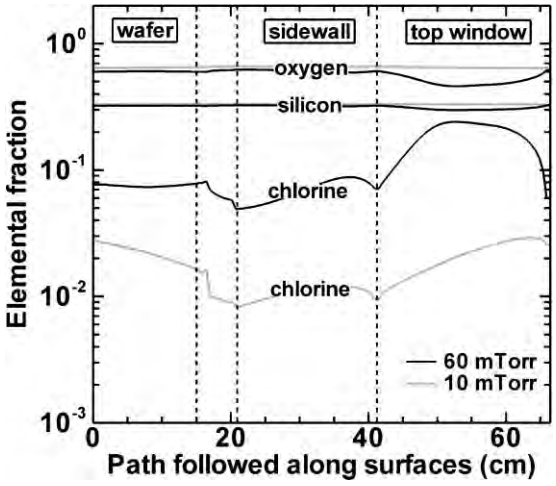

Figure 13. Calculated chemical composition of the deposited film for 10 and 60 mTorr chamber pressure. The other operating conditions are the same as in the beginning of the results and discussion section. The *x*-axis corresponds to the dashed arrow path illustrated in Figure 1.

underestimated as explained in the previous paragraphs, we still can obtain valuable information on flux uniformity on the other reactor surfaces. At 60 mTorr, the O flux is generally more than an order of magnitude lower compared to the 10 mTorr case. The lower O flux can be explained by the lower dissociation degree, as the electrons have lost more energy by vibrational and rotational excitation collisions. This lower flux gives rise to a more modest oxidation of the silicon chloride film, as was also the case at lower operating power. Indeed, the Cl content in the SiO_2 film is around 11% at the wafer and sidewall, increasing even to 33% at the top window, at 60 mTorr, whereas it is only a few % at 10 mTorr, as shown in Figure 13. Hence, at the top window, the layer is clearly not SiO_2-like, as it contains almost as much chlorine as oxygen (28% Si, 39% O, and 33% Cl) which is undesirable in terms of chemical stability of the deposited film.[4] Moreover, since the coating under this condition contains much more chlorine, it is more receptive to chemical etching by chlorine radicals. Indeed, it was found that the chemical etch rate was 13% of the total deposition rate, which is a significant increase compared to the case at 10 mTorr where chemical etching was negligible.

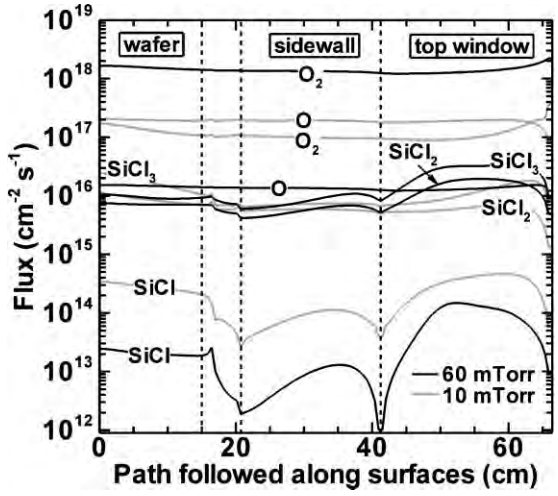

Figure 12. Calculated fluxes of the relevant neutral species for SiO_2 film deposition at 10 and 60 mTorr chamber pressure. The other operating conditions are the same as in the beginning of the results and discussion section. The *x*-axis corresponds to the dashed arrow path illustrated in Figure 1.

It can therefore be concluded that a higher pressure seems to have negative effects on the chemical composition of the film, certainly at the top window, due to significantly more incorporated chlorine in the SiO_2-like coating.

5. Conclusion

We investigated the PECVD process of a SiO_2 coating by $SiCl_4/O_2/Ar$ ICPs applied in wafer processing reactors by means of a hybrid model. Thickness measurements were performed on the wafer for validation of the model. A reaction set for the bulk plasma and surface chemistry was created for $Ar/SiCl_4/O_2$ ICPs and presented in this paper.

The properties of the deposited SiO_2 layer, including chemical composition, thickness, and overall uniformity

Plasma Process. Polym. **2013,** *10*, 714–730

DOI: 10.1002/ppap.201300005

on all reactor surfaces, are discussed. Furthermore, the deposition characteristics are explained, by analyzing some general bulk plasma properties, such as the species densities and their leading production and loss processes, as calculated by the model. Furthermore, the effects of gas flow; operating power and chamber pressure at a fixed gas ratio were investigated, to obtain more insight in how to improve the general properties of the deposited SiO_2 film.

The most important precursors for deposition appear to be $SiCl_3$, $SiCl_2$, and SiCl, while sputtering of the layer by ions is found to be negligible, as no bias is applied. O and O_2 are the most important species for oxidation of the film to form a SiO_2 coating. Gas phase oxidation of the $SiCl_x$ precursors was found to be negligible, indicating that the layer growth mechanism is based on the deposition of $SiCl_x$ species, followed by surface oxidation towards SiO_2.

The calculated chemical composition of the deposited film was found to be very similar on all reactor surfaces and very close to stoichiometric SiO_2 at the operating conditions investigated, except at low power and high pressure. Indeed, the percentage chlorine in the coating was typically found in the order of 1–3%, but it increases to ~7% at low power (200 W), and even to ~33% at the top window, at a pressure of 60 mTorr. Such a high percentage of chlorine in the film is undesirable in terms of chemical stability of the film.

The calculated thickness of the coating was found to vary significantly along the reactor surfaces, depending on the conditions. At 400 sccm total gas flow, 1 200 W and 10 mTorr gas pressure, the thickness ranges from 20–50 nm at the sidewall to 300 and 420 nm at the center of the wafer and near the gas nozzle, respectively.

By varying the total gas flow, the spreading of deposition precursors in the reactor volume can be tuned for controlling the overall deposition rate and hence the thickness of the coating. A lower gas flow results in a thinner coating, but the thickness uniformity was not affected.

At lower operating power, the gases are less dissociated, resulting in a lower density and flux of deposition precursors and hence a thinner SiO_2 film. Furthermore, the thickness uniformity is significantly improved, because of a more uniform plasma shape, but as mentioned above, the chlorine content in the film was found to be higher (~7% at 200 W vs. ~1% at 1 200 W), due to the more modest oxidation of the layer.

Finally, at higher pressure, the experiment and the model show contradictory results concerning the thickness uniformity. It was found that the model underestimates the coating thickness on the wafer due to a limitation in local nozzle gas flow towards the center of the wafer under this condition. Nevertheless, still valuable information could be derived from the modeling results. At higher pressure, the film tends to contain significantly more chlorine, which is generally undesired for the chemical stability of the coating.

In general, it can be concluded that "mild" operating conditions, especially low operating power, can enhance the plasma uniformity and hence the coating thickness uniformity along the reactor surfaces. A higher pressure can most probably improve thickness uniformity on the sidewall and top window of the reactor, but yields a coating with more chlorine incorporated, which is detrimental for the chemical stability of the film. Hence, under the studied conditions, a trade-off exists between film uniformity on the one hand, and film composition on the other hand. Depending on the application, one needs to find the desired balance between film uniformity and chlorine content in the layer. This research has shown that the structural and chemical state of the coating significantly depends on the operating conditions and it is clearly not always uniform along the reactor surface. Therefore, process parameters must be carefully chosen, to ensure a good uniformity of the coating for eventually obtaining more uniform plasma.

Acknowledgements: The Fund for Scientific Research Flanders (FWO) is acknowledged for financial support of this work. The authors thank M. Kushner for providing the code and E. Altamirano-Sánchez from IMEC for useful advice. This work was carried out in part using the Turing HPC infrastructure at the CalcUA core facility of the Universiteit Antwerpen, a division of the Flemish Supercomputer Center VSC, funded by the Hercules Foundation, the Flemish Government (department EWI) and the University of Antwerp.

Received: January 10, 2013; Revised: April 2, 2013; Accepted: April 14, 2013; DOI: 10.1002/ppap.201300005

Keywords: coatings; PECVD; plasmas; simulations; SiO_2

[1] G. Cunge, B. Pelissier, O. Joubert, R. Ramos, C. Maurice, *Plasma Sources Sci. Technol.* **2005**, *14*, 599.
[2] S. J. Ullal, A. R. Godfrey, E. Edelberg, L. Braly, V. Vahedi, E. S. Aydil, *J. Vac. Sci. Technol. A* **2002**, *20*, 43.
[3] A. R. Godfrey, S. J. Ullal, L. Braly, E. Edelberg, V. Vahedi, E. S. Aydil, *Review Of Sci. Instr.* **2001**, *72*, 3260.
[4] J. C. Alonso, R. Vasquez, A. Ortiz, V. Pankov, E. Andrade, *J. Vac. Sci. Technol. A* **1998**, *16*, 3211.
[5] A. Ortiz, C. Falcony, M. Farias, L. Cota-Araiza, G. Soto, *Thin Solid Films* **1991**, *206*, 6.
[6] J. C. Alonso, E. Pichardo, L. Rodriguez-Fernandes, J. C. Cheang-Wong, A. Ortiz, *J. Vac. Sci. Technol. A* **2001**, *19*, 507.
[7] A. Ortiz, S. Lopez, C. Falcony, M. Farias, L. Cota-Araiza, G. Soto, *J. Elec. Mat.* **1990**, *19*, 1411.
[8] M. J. Kushner, **2009**, *J. Phys. D Appl. Phys. 42*, 194013.
[9] C. R. Moylan, S. B. Green, J. I. Brauman, *Int. J. Mass Spectrom. Ion Process.* **1990**, *96*, 299.

[10] A. M. Efremov, D. P. Kim, C. I. Kim, *Vacuum* **2004**, *75*, 237.
[11] I. G. Kouznetsov, A. J. Lichtenberg, M. A. Lieberman, *Plasma Sources Sci. Technol.* **1996**, *5*, 662.
[12] I. A. Kossyi, A. Y. Kostinsky, A. A. Matveyev, V. P. Silakov, *Plasma Sources Sci. Technol.* **1992**, *1*, 207.
[13] E. G. Thorsteinsson, J. T. Gudmundsson, *Plasma Sources Sci. Technol.* **2010**, *19*, 055008.
[14] G. Cunge, N. Sadeghi, R. Ramos, *J. Appl. Phys.* **2007**, *102*, 093305.
[15] P. Kleinert, D. Schmidt, J. Kirchhof, A. Funke, *Kristall Techn.* **1980**, *15*, 85.
[16] P. Subramonium, M. J. Kushner, *J. Vac. Sci. Technol. A* **2002**, *20*, 325.
[17] K. Becker, J. Mahoney, M. Gutkin, V. Tarnovsky, R. Basner, *Jap. J. Appl. Phys.* **2006**, *45*, 8188.
[18] R. Basner, M. Gutkin, J. Mahoney, V. Tarnovsky, H. Deutch, K. Becker, *J. Chem. Phys.* **2005**, *123*, 054313.
[19] M. Gutkin, J. M. Mahoney, V. Tarnovsky, H. Deutch, K. Becker, *Int. J. Mass. Spec.* **2009**, *280*, 101.
[20] J. Mahoney, V. Tarnovsky, K. H. Becker, *Eur. Phys. J. D* **2008**, *46*, 289.
[21] K. N. Joshipura, B. G. Vaishnav, S. Gangopadhyay *Int. J. Mass Spectrom.* **2007**, *261*, 146.
[22] K. Tachibana, *Phys. Rev. A* **1986**, *34*, 1007.
[23] C. Hsu, M. A. Nierode, J. W. Coburn, D. B. Graves, *J. Phys. D Appl. Phys.* **2006**, *39*, 3272.
[24] S. Rauf, M. J. Kushner, *J. Appl. Phys.* **1997**, *82*, 2805.
[25] S. Panda, D. J. Economou, M. Meyyappan, *J. Appl. Phys.* **2000**, *87*, 8323.
[26] B. Eliasson, M. Hirth, U. Kogelschatz, *J. Phys. D Appl. Phys.* **1987**, *20*, 1421.
[27] D. Husain, P. E. Norris, *J. Chem. Soc. Faraday Trans.* **1978**, *2*, 74.
[28] G. Cunge, D. Vempaire, R. Ramos, M. Touzeau, O. Joubert, P. Bodard, N. Sadeghi, *Plasma Sources Sci. Technol.* **2010**, *19*, 034017.
[29] S. D. Le Picard, A. Canosa, D. Reignier, T. Stoecklin, *Phys. Chem. Chem. Phys.* **2002**, *4*, 3659.
[30] M. J. Kushner, *J. Appl. Phys.* **1993**, *74*, 6538.
[31] D. H. Kim, G. H. Lee, S. Y. Lee, D. H. Kim, *J. Cryst. Growth* **2006**, *286*, 71.
[32] M. W. Kielbauch, D. B. Graves, *J. Vac. Sci. Technol. A* **2003**, *21*, 116.
[33] R. J. Hoekstra, M. J. Grapperhaus, M. J. Kushner, *J. Vac. Sci. Technol. A* **1997**, *15*, 1913.
[34] *Lam Research Corporation* www.lamrc.com.
[35] F. Denes, Z. Q. Hua, C. E. C. A. Hop, R. A. Young, *J. Appl. Pol. Sci.* **1996**, *61*, 875.
[36] T. Sakurai, S. Kobayashi, J. Ogura, Y. Inoue, H. Hori, *Aust. J. Phys.* **1995**, *48*, 515.
[37] L. M. Blinov, A. G. Golovkin, L. I. Kaganov, V. B. Oparin, A. A. Razhavski, A. M. Shterenberg, V. V. Volodko, V. I. Zyn, *Plasma Chem. Plasma Proc.* **1998**, *18*, 509.
[38] W. ZhaoKui, L. KuiXun, L. YanHui, L. XuanYing, Z. ZuSong, *Chin. Phys.* **2006**, *15*, 2374.
[39] W. ZhaoKui, L. YanHui, *J. Mater. Sci.* **2007**, *42*, 9920.
[40] K. Takechi, M. A. Lieberman, *J. Appl. Phys.* **2001**, *90*, 3205.
[41] S. Tinck, W. Boullart, A. Bogaerts, *Plasma Sources Sci. Technol.* **2011**, *20*, 045012.

DOI: 10.1002/ppap.201300005